Trickle-Bed Reactor Model for Desulfurization and Dearomatization of Diesel

R. Chowdhury
Food Technology and Biochemical Engineering Dept., Jadavpur University, Calcutta 700 032, India

E. Pedernera and R. Reimert
Engler-Bunte-Institut der Universität Karlsruhe(TH), Bereich Gas, Erdöl und Kohle
D-76131, Karlsruhe, Germany

Desulfurization and hydrogenation of aromatics in diesel oil were investigated in an isothermally operated trickle-bed reactor 500 mm long and with a 19-mm ID, using commercial bifunctional $NiMo/Al_2O_3$ catalysts. The operating temperature, pressure, liquid hourly space velocity, gas/oil ratio, and the initial concentration of H_2S were 300–380°C, 2–8 MPa, 1–4 h^{-1}, 100–500 $m^3_{NTP)}/m^3$ and 0–8 vol %, respectively. The increase in pressure and decrease in liquid hourly space velocity lead to deeper desulfurization and hydrogenation of both aromatics. Although a higher gas-to-oil ratio and lower initial concentration of H_2S enhance the desulfurization reaction, these parameters play almost no role for hydrogenation. Desulfurization increases sharply with increased temperature, but with the same change in temperature the conversion of aromatics increases only up to 360°C, above which it falls sharply. This behavior is explained by the approaching of chemical equilibria by the reversible hydrogenation reactions of the aromatics at higher temperatures. A mechanistic mathematical model was developed for a two-phase flow reactor, considering both mass transfer and chemical reaction in the reactor. The kinetic equations for desulfurization and for the hydrogenation of mono-, di- and polyaromatics were established. Simulated results are compared satisfactorily with the experimental observations.

Introduction

Reduction of SO_2 emissions and volatile organic matter (VOM) during the combustion of diesel oil is necessary to reduce pollution. As a consequence, the refineries are under heavy pressure to reduce the sulfur and aromatics content of diesel oil in the near future (Ertl et al., 1996). Table 1 tabulates the sulfur and aromatic content of diesel oil in Europe.

Table 1. Requisite Values of Sulfur and Aromatic Contents of Diesel Oil in Europe

Year	*S* (ppm)	Aromatics (Vol %)
1994	1,000–3,000	25–35
2000–02	200	10–20

Correspondence concerning this article should be addressed to R. Chowdhury.

Catalytic hydrogenation of diesel oil is one of the promising possibilities. To achieve this goal with a low consumption of hydrogen, a proper understanding of the influence of the operating parameters is necessary. A number of studies (Girgis and Gates, 1991; van den Berg et al., 1993; Ma et al., 1994, 1995; Andari et al., 1996) on the determination of the kinetics and of the mechanisms of desulfurization of diesel oil based on the model components like benzothiophene and dibenzothiophene have been reported. The desulfurization kinetics of the model components cannot, however, be used to predict the kinetics of the desulfurization of diesel oil.

It is evident from the literature (Matarrese et al., 1983; Suchanek, 1990; Girgis and Gates, 1991; Cooper et al., 1992, 1993; Stanislaus and Cooper, 1994) that under normal hydrogenation conditions, high conversion of aromatics, especially that of monoaromatics, is hardly achievable in the presence of the conventional catalysts (CoMo(/NiMo/NiW)/Al_2O_3).

Some of the investigators (Cooper and Stanislaus, 1993) therefore recommend the use of rare earth metal as a catalyst in the second stage of a two-stage catalytic process to hydrogenate the aromatics completely. The first stage of this process is a conventional catalytic desulfurization of diesel oil. The temperature and pressure needed in the second stage are low.

A mechanistic mathematical model is necessary to scale-up the laboratory data to commercial scale. Although a three-phase model of the desulfurization of vacuum gas oil has been reported by Korsten and Hoffmann (1996), such a model for normal diesel oil, whose evaporation cannot be neglected, at least at the entrance of the reactor, has not yet been reported. The kinetics of hydrogenation of individual aromatic compounds in diesel oil, namely, benzene (Sharma et al., 1993) and naphthalene (Huang and Kang, 1995), have been reported. Although a few pioneering works (Quann and Jaffe, 1992, 1996; Korre et al., 1994; Stanislaus and Cooper, 1994) have been reported on the kinetics and mechanistic evaluation of complex polynuclear aromatic mixtures of petroleum compounds, it is still necessary to develop a generalized model for a reactor undergoing the hydrogenation of aromatics along with desulfurization of diesel oil.

In the present investigation, the kinetics of parallel desulfurization and the dearomatization of diesel oil have been studied using a cocurrently fed trickle-bed reactor utilizing $NiMo/Al_2O_3$ as the catalyst. A mathematical model for the desulfurization and dearomatization of diesel oil has been developed.

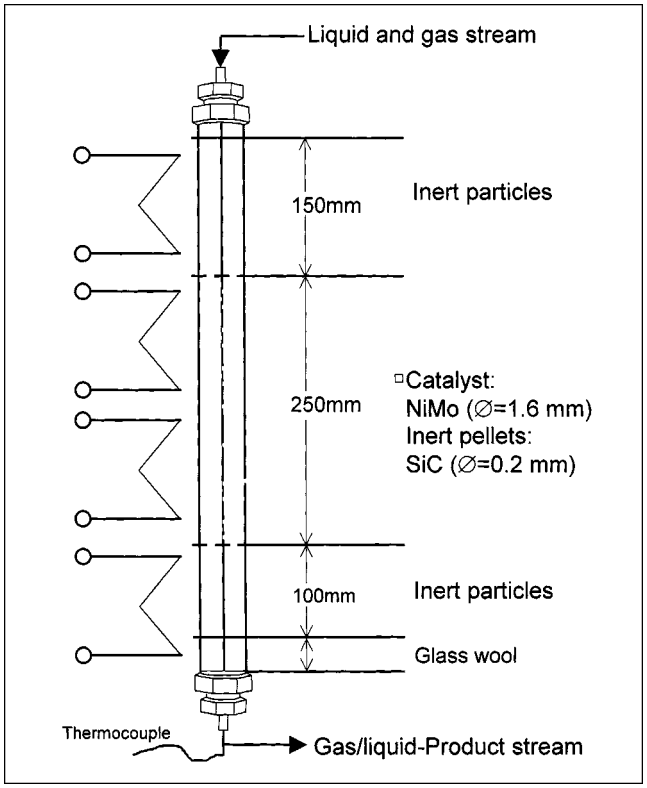

Figure 1. Reactor.

Experimental Studies

Materials

Feed Oil. The properties of the diesel oil used in the present investigation are shown in Table 2.

Catalyst. The catalyst (CRITERION 424) used in the present investigation is shaped like a trilobe. It has a diameter of 1.6 mm, a length of 3.5 mm, and a bulk density of 820 kg/m^3. γ-Alumina is the support, molybdenum is the catalytic material, and nickel acts as promotor. In its oxidized form, the catalyst has the following composition: NiO: 4 wt %, MoO: 19.5 wt %, P_2O_5: 8 wt %; Al_2O_3: 68.5 wt %.

Equipment and procedure

The trickle-bed reactor used for the experiments has a diameter of 19 mm and is 500 mm long. It is shown in Figure 1.

Table 2. Properties of Feed Diesel Oil

Distillation Curve (ASTM D2887)	Aromatics and Naphthenes (ASTM 2549-ASTM 3239) Components	Content (wt %)
IBP (0.5) vol. %): 180°C	Total Aromatics:	33.50
50 vol %: 337°	Monoaromatics:	17.96
FBP (99.5 vol %): 434°C	Diaromatics:	8.77
S (ppm): 16,298	Triaromatics:	1.64
N (ppm): 218	Tetraaromatics:	0.95
Density: 865 kg/m^3	Unidentified:	4.19
	Naphthenes:	19.25

About 250 mm of the reactor length was filled with catalyst and a diluent, silicon carbide, mixed in a ratio of 1:1.25 (vol/vol). The diluent's diameter lies in the 0.17–0.22 mm range. The parts over (150 mm) and under (100 mm) the catalytically active zone of the reactor were filled with silicon carbide only. An efficient heat transfer from the heated wall to the fluid was thus ensured. The other important effect of the inert material was the uniform distribution (Al-Dahhan and Dudukovic, 1996) of the fluid flowing over a cross section of the reactor. The porosity of the bed was 0.5. Before the actual experimental runs, the catalyst was transformed into the active sulfide form by following the method suggested by the manufacturer of the catalyst, that is, passing feed diesel oil containing dimethyl disulfide over the catalyst.

The diesel oil was brought to the reaction pressure with the help of a metering pump, and was mixed with gaseous reactant consisting either of pure hydrogen or a mixture of hydrogen/hydrogen sulfide. The gas–oil mixture was heated and was led to the reactor. An isothermal condition was maintained in the reactor by four temperature-controlled heaters. After leaving the reactor, the pressure of the gas-oil mixture was reduced to atmospheric pressure by a needle valve. After cooling and separation from the liquid phase, the gas phase was directed to a flask containing sodium hydroxide solution to neutralize hydrogen sulfide. Liquid samples were taken and were analyzed to determine the sulfur and aromatics content. The experimental results are thus of the integral reactor type.

Experiments have been performed to investigate the effects of the different reactor parameters, namely, tempera-

Table 3. Details of Experimental Runs

Run No.	Temp. (°C)	Pres. MPa	LHSV h^{-1}	$Q_{g,\mathrm{NTP}}/Q_l$ m^3/m^3	y_{H_2S} vol.%
T-1	**300**	4	2	200	1.4
T-2	**320**	4	2	200	1.4
T-3	**340**	4	2	200	1.4
T-4	**360**	4	2	200	1.4
T-5	**380**	4	2	200	1.4
P-1	320	**2**	2	200	1.4
P-2	320	**4**	2	200	1.4
P-3	320	**6**	2	200	1.4
P-4	320	**8**	2	200	1.4
L-1	320	4	**1**	200	1.4
L-2	320	4	**2**	200	1.4
L-3	320	4	**3**	200	1.4
L-4	320	4	**4**	200	1.4
Q-1	320	4	2	**100**	1.4
Q-2	320	4	2	**200**	1.4
Q-3	320	4	2	**300**	1.4
Q-4	320	4	2	**400**	1.4
Q-5	320	4	2	**500**	1.4
H_2S-1	320	4	2	200	**0.0**
H_2S-2	320	4	2	200	**1.4**
H_2S-3	320	4	2	200	**3.0**
H_2S-4	320	4	2	200	**5.0**
H_2S-5	320	4	2	200	**8.0**

Note: T-: Experiments to study the effect of temperature; P-: experiments to study the effect of pressure; L-: experiments to study the effect of LHSV; Q-: experiments to study the effect of $Q_{g,NTP}/Q_l$; H_2S: experiments to study the effect of y_{H_2S}.

ture, pressure, Q_g/Q_l ratio, and the initial concentration of H_2S. Experimental details are given in Table 3.

Analytical

Chemicals. Silica gel (Aldrich Chemie, 100–200 mesh), Al_2O_3 (Acros Organics, New Jersey, 50–200 μm), diethyl ether (0.0075% H_2O, Merck) and chloroform (Merck) were used.

Determination of Sulfur Content. The sulfur content of diesel oil before and after desulfurization was determined using an energy-dispersive X-ray fluorescence spectrophotometer (Oxford Lab X 300). Each sample was purged with nitrogen before the analysis to make it free from dissolved hydrogen sulfide.

Determination of Aromatic Content: Total Aromatics. The total aromatic content was determined by elution chromatography (D-2549). About 600 mm of the column was filled with silica gel. The portion above this was filled with alumina instead of bauxite because none of the latter of the recommended quality was available. Alumina was activated by placing it in a furnace at a temperature of 538°C for 16 h. The alumina was cooled to room temperature before being introduced into the glass column. Diethyl ether, *n*-pentane, and chloroform were used as the solvents. Before each analysis, the bed was freshly prepared to avoid the effects of the oil residue on it.

Determination of Aromatic Content: GC-MS Analysis. After the separation of the aromatic part from the nonaromatic part, the former was analyzed with a gas-chromatograph mass spectrometer (MS). Helium was used as the carrier gas. The ionization in the MS was done with an electron field of 70 eV. The signals from the MS were processed with a FORTRAN program (ASTM D-3239-91) to determine the concentration of different types (mono-, di-, poly-) of aromatics. The nonaromatic part of the original diesel fed to the reactor was analyzed using the ASTM D-2425-93 method to determine the initial content of the naphthenes.

Formulation of Mathematical Model

The mathematical model has been developed with the following assumptions:

1. The reactor operates isothermally under isobaric and steady-state conditions.
2. There is no radial profile of concentration within the reactor.
3. The reactor behaves like a plug-flow reactor (Levenspiel, 1982), as the dispersion group determined for the reactor is 0.0025.
4. Evaporation of diesel oil occurs instantaneously only at the entrance of the reactor. The evaporation of the reacting components can be neglected due to their high molecular weights.
5. Mass-transfer resistance lies in the gas–liquid interface. The mass-transfer resistance at the liquid–solid interface and the resistance to pore diffusion can be neglected (Valerius et al., 1996).
6. The gas and the liquid phases are in equilibrium at their interface.
7. The desulfurization reaction occurs in the following manner:

$$\text{Ar-S} + 2\,H_2 \rightarrow \text{Aromat} + H_2S, \qquad \text{(I)}$$

and is irreversible under normal hydrotreating conditions.

8. The adsorption coefficient, k_{ad} of the H_2S does not depend on temperature.
9. The aromatics consist of three groups, namely mono-, di-, and polyaromatics. Tri-, tetra-, and penta-aromatics belong to the polyaromaic group. All the polyaromatics behave like triaromatic.
10. Each of the aromatic groups undergoes different hydrogenation reactions that are all reversible under normal hydrogenation conditions. Some of the representative reactions may be as follows (Jaffe, 1974):

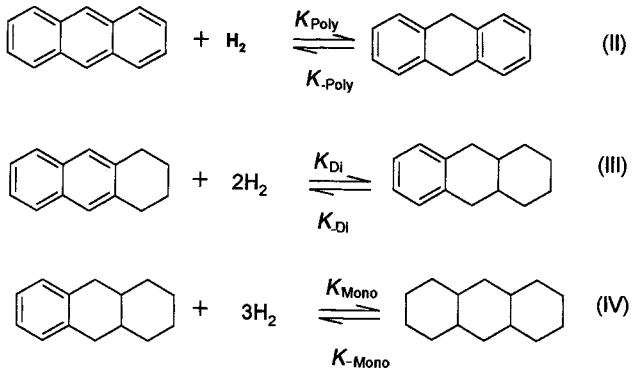

In the generalized form the hydrogenation reactions can be represented in the following way:

$$\text{Polyaromatic} + \text{H}_2 \underset{k_{-\text{Poly}}}{\overset{k_{\text{Poly}}}{\rightleftharpoons}} \text{diaromatic} \qquad \text{(IIa)}$$

$$\text{Diaromatic} + 2\text{H}_2 \underset{k_{\text{-Di}}}{\overset{k_{\text{Di}}}{\rightleftharpoons}} \text{monoaromatic} \qquad \text{(IIIa)}$$

$$\text{Monoaromatic} + 3\text{H}_2 \underset{k_{-\text{Mono}}}{\overset{k_{\text{Mono}}}{\rightleftharpoons}} \text{naphthene} \qquad \text{(IVa)}$$

11. The forward reactions are pseudo first order with respect to the aromatics only as the hydrogen has been used in excess (Girgis and Gates, 1991; Wilson and Kriz, 1984).

12. The backward reactions of the reversible hydrogenation reactions of aromatics are first order with respect to the products (Wilson and Kriz, 1984).

13. The heat of the reactions of the aromatics hydrogenation reaction is 67 kJ/mol of hydrogen (Stanislaus and Cooper, 1994).

14. The catalyst particles are completely wetted (Sie, 1991).

15 Both the gaseous and the liquid phases may flow through the entire void space in the reactor.

The following form of the Langmuir-type rate equation has been considered for the desulfurization reaction:

$$r_{\text{Ar-S}} = -\frac{kC_{\text{Ar-S}}^{m_1} C_{\text{H}_2}^{m_2}}{1 + k_{ad} C_{\text{H}_2\text{S}}}. \qquad (1)$$

As explained in assumption 3, the reactor follows plug-flow behavior. Therefore, reaction rates, $r_{\text{Ar-S}}$, have been evaluated at different values of sulfur conversions, $X_{\text{Ar-S}}$, by differential analysis of the experimental data (Levenspiel, 1982) obtained from the currently operated integral trickle-bed reactor. The adsorption coefficient, k_{ad}, has been evaluated from the experimental data obtained by varying the initial concentration of H_2S from 0–8 vol % at constant temperature (320°C), pressure (4 MPa), and $Q_{g(\text{NTP})}/Q_l$ ratio (200) using the method of least square. These valves and expressions are given in Table 4. Reaction orders, m_1, m_2, and reaction rate constants, k, have been determined using the experimental data obtained by regression analysis at 320°C with varying pressures (2–8 MPa) and liquid hourly space velocity (LHSV) (1–4 h^{-1}). The values of m_1 and m_2 are 1.6 and 0.56, respectively. The reaction rate constants, k, at other temperatures also have been determined by nonlinear regression analysis of the experimental data. The temperature dependencies of all the reaction rate constants have been described by the Arrhenius law. Activation energies and the preexponential factors also have been determined by regression analysis and are tabulated in Table 4.

Table 4. Reaction and Adsorption Rate Constants

Reaction Rate Constants	Expression
k_{ad}	50,000
k	$2.5\times10^{12}\exp(-19{,}384/T)$
k^*_{Mono}	$6.04\times10^{2}\exp(-12{,}414/T)$
k^*_{Di}	$8.5\times10^{2}\exp(-12{,}140/T)$
k^*_{Poly}	$2.66\times10^{5}\exp(-15{,}170/T)$

The following rate equations have been used to describe the hydrogenation of aromatics:

II:

$$r_{\text{Poly}} = -k_{\text{Poly}} C_{\text{Poly}} P_{\text{H}_2}^{n3} + k_{-\text{Poly}} C_{Di} \qquad (2)$$

III:

$$r_{\text{Di}} = -k_{\text{Di}} C_{\text{Di}} P_{\text{H}_2}^{n2} + k_{-\text{Di}} C_{\text{Mono}} \qquad (3)$$

IV:

$$r_{\text{Mono}} = -k_{\text{Mono}} C_{\text{Mono}} P_{\text{H}_2}^{n1} + k_{-\text{Mono}} C_{\text{Naph}} \qquad (4)$$

$$r_{\text{Naph}} = k_{\text{Mono}} C_{\text{Mono}} P_{\text{H}_2}^{n1} - k_{-\text{Mono}} C_{\text{Naph}}. \qquad (5)$$

As $(P_{\text{H}_2})^{n1}$, $(P_{\text{H}_2})^{n2}$, and $(P_{\text{H}_2})^{n3}$ are constant when the reaction pressure was held constant, applying assumption 11, Eqs. 2–4 reduce to the following equations:

$$r_{\text{Poly}} = -k^*_{\text{Poly}} C_{\text{Poly}} + k_{-\text{Poly}} C_{\text{Di}} \qquad (6)$$

$$r_{\text{Di}} = -k^*_{\text{Di}} C_{\text{Di}} + k_{-\text{Di}} C_{\text{Mono}} \qquad (7)$$

$$r_{\text{Mono}} = -k^*_{\text{Mono}} C_{\text{Mono}} + k_{-\text{Mono}} C_{\text{Naph}}, \qquad (8)$$

where,

$$k^*_{\text{Poly}} = k_{\text{Poly}} P_{\text{H}_2}^{n3} \qquad (9)$$

$$k^*_{\text{Di}} = k_{\text{Di}} P_{\text{H}_2}^{n2} \qquad (10)$$

$$k^*_{\text{Mono}} = k_{\text{Mono}} P_{\text{H}_2}^{n1}. \qquad (11)$$

To determine the rate constants for the backward reactions, dynamic equilibrium constants have been defined as follows:

$$K_{\text{Poly}} = \frac{k^*_{\text{Poly}}}{k_{-\text{Poly}}} \qquad (12)$$

$$K_{\text{Di}} = \frac{k^*_{\text{Di}}}{k_{-\text{Di}}} \qquad (13)$$

$$K_{\text{Mono}} = \frac{k^*_{\text{Mono}}}{k_{-\text{Mono}}}. \qquad (14)$$

By the use of the van't Hoff correlation (Eq. 15), the dynamic equilibrium constants at different temperatures have been determined.

$$\frac{d(\ln K_{\text{Poly/Di/Mono}})}{dT} = \frac{\Delta H_{\text{Poly/Di/Mono}}}{RT^2}. \qquad (15)$$

After determining the reaction rate constants for the forward reactions at different pressures at a constant temperature of 320°C, the exponents $n1$, $n2$, and $n3$ were determined by regression analysis, yielding, $n1 = 1$ and $n2 = n3 = 0.5$.

The temperature dependencies of the forward reactions have been considered to be governed by Arrhenius law. The activation energies and the preexponential factors have been determined by regression analysis and are tabulated in Table 4.

Model equations

The following differential mass-balance equations have been obtained for different components for different phases.

Gas Phase. For 0 mm $\le z \le$ 500 mm

$$\frac{dP_{H_2}}{dz} = -\frac{RT}{u_g \epsilon} k^l_{H_2} a_p \left(\frac{P_{H_2}}{H_{H_2}} - C^l_{H_2} \right) \tag{16}$$

$$\frac{dP_{H_2S}}{dz} = -\frac{RT}{u_g \epsilon} k^l_{H_2S} a_p \left(\frac{P_{H_2S}}{H_{H_2S}} - C^l_{H_2S} \right). \tag{17}$$

Liquid Phase. For nonreactive zones, that is, for 0 mm $\le z \le$ 150 mm and 400 mm $\le z \le$ 500 mm:

$$\frac{dC^l_{H_2}}{dz} = \frac{k^l_{H_2} a_p}{u_l \epsilon} \left(\frac{P_{H_2}}{H_{H_2}} - C^l_{H_2} \right) \tag{18}$$

$$\frac{dC^l_{H_2S}}{dz} = \frac{k^l_{H_2S} a_p}{u_l \epsilon} \left(\frac{P_{H_2S}}{H_{H_2S}} - C^l_{H_2S} \right). \tag{19}$$

For the reactive zone, that is, 150 mm $\le z \le$ 400 mm:

$$\frac{dC^l_{H_2}}{dz} = \frac{k^l_{H_2} a_p}{u_l \epsilon} \left(\frac{P_{H_2}}{H_{H_2}} - C^l_{H_2} \right) + \frac{\rho_b \xi}{u_l \epsilon} \left(2^* r_{\text{Ar-S}} + r_{\text{Poly}} + 2^* r_{\text{Di}} + 3^* r_{\text{Mono}} \right) \tag{20}$$

$$\frac{dC^l_{H_2S}}{dz} = \frac{k^l_{H_2S} a_p}{u_l \epsilon} \left(\frac{P_{H_2S}}{H_{H_2S}} - C^l_{H_2S} \right) - \frac{\rho_b \xi}{u_l \epsilon} r_{\text{Ar-S}} \tag{21}$$

$$\frac{dC_{\text{Ar-S}}}{dz} = \frac{\rho_b \xi}{u_l \epsilon} r_{\text{Ar-S}} \tag{22}$$

$$\frac{dC_{\text{Poly}}}{dz} = \frac{\rho_b \xi}{u_l \epsilon} r_{\text{Poly}} \tag{23}$$

$$\frac{dC_{\text{Di}}}{dz} = \frac{\rho_b \xi}{u_l \epsilon} (r_{\text{Di}} - r_{\text{Poly}}) \tag{24}$$

$$\frac{dC_{\text{Mono}}}{dz} = \frac{\rho_b \xi}{u_l \epsilon} (r_{\text{Mono}} - r_{\text{Di}}) \tag{25}$$

$$\frac{dC_{\text{Naph}}}{dz} = -\frac{\rho_b \xi}{u_l \epsilon} r_{\text{Mono}}. \tag{26}$$

The mass transfer coefficients $k^l a_p$ and Henry's constants have been determined using several empirical expressions (Korsten and Hoffmann, 1996). The density of diesel oil at different reaction conditions, and the flow rates of liquid and gas phases after the partial evaporation of diesel oil at the entrance, have been determined using the ASPEN-PLUS simulation program (Redlich-Kong-Soaves state equation and API method for the molar volume of liquid phase). The expressions given by Eqs. 1 and 6 through 8 have been used to replace $r_{\text{Ar-S}}$, r_{Mono}, r_{Di}, and r_{Poly} in Eqs. 20 through 26. The model equations (Eqs. 16–26) have been solved with a FORTRAN program for fourth-order Runge-Kutta method using the following initial conditions: At $z = 0$

$$\begin{pmatrix} P_{H_2} = P_{H_2,0} \\ P_{H_2S} = P_{H_2,0} \\ C^l_{H_2} = 0 \\ C^l_{H_2S} = 0 \\ C_{\text{Ar-S}} = C_{\text{Ar-S},0} \\ C_{\text{Poly}} = C_{\text{Poly},0} \\ C_{\text{Di}} = C_{\text{Di},0} \\ C_{\text{Mono}} = C_{\text{Mono},0} \\ C_{\text{Naph}} = C_{\text{Naph},0} \end{pmatrix} \tag{26a}$$

The fractions of Ar-S and the mono-, di-, and poly- aromatics, converted through different hydrogenation reactions, have been calculated using the following expressions:

$$x_{\text{Ar-S}} = \frac{C_{\text{Ar-S},0} - C_{\text{Ar-S}}}{C_{\text{Ar-S},0}} \tag{27}$$

$$X_{\text{Poly}} = \frac{C_{\text{Poly},0} - C_{\text{Poly}}}{C_{\text{Poly},0}} \tag{28}$$

$$X_{\text{Di}} = \frac{C_{\text{Di},0} - C_{\text{Di}}}{C_{\text{Di},0}} \tag{29}$$

$$X_{\text{Mono}} = \frac{C_{\text{Mono},0} - C_{\text{Mono}}}{C_{\text{Mono},0}} \tag{30}$$

$$X_{\text{Tot}} = \frac{C_{\text{Tot},0} - (C_{\text{Poly}} + C_{\text{Di}} + C_{\text{Mono}})}{C_{\text{Tot},0}}. \tag{31}$$

The equilibrium conversion for all the aromatic components has been determined with the aid of the following equations. At equilibrium,

$$r_{\text{Mono}} = r_{\text{Di}} = r_{\text{Poly}} = 0. \tag{32}$$

Therefore, using Eqs. 6 through 14,

$$C_{\text{Poly,e}} = \frac{1}{K_{\text{Poly}}} C_{\text{Di,e}} \tag{33}$$

$$C_{\text{Di,e}} = \frac{1}{K_{\text{Di}}} C_{\text{Mono,e}}, \tag{34}$$

and using Eqs. 33 and 34,

$$C_{\text{Poly,e}} = \frac{1}{K_{\text{Di}} K_{\text{Poly}}} C_{\text{Mono,e}} \tag{35}$$

$$C_{\text{Mono,e}} = \frac{1}{K_{\text{Mono}}} C_{\text{Naph,e}}. \tag{36}$$

Again, by making the total molar balance of aromatics and naphthenes,

$$C_{\text{Tot,0}} + C_{\text{Naph,0}} = C_{\text{Mono},e} + C_{\text{Di},e} + C_{\text{Poly},e} + C_{\text{Naph},e}. \tag{37}$$

Therefore,

$$C_{\text{Naph},e} = C_{\text{Naph,0}} + C_{\text{Tot,0}} - C_{\text{Tot},e}, \tag{38}$$

where

$$C_{\text{Tot},e} = C_{\text{Mono},e} + C_{\text{Di},e} + C_{\text{Poly},e}. \tag{39}$$

Substituting the expression for $C_{\text{Naph},e}$ from Eqs. 37 and 38 and those for $C_{\text{Di},e}$ and $C_{\text{poly},e}$ from Eqs. 34 and 35 in Eq. 36,

$$C_{\text{Mono},e} = \frac{C_{\text{Tot,0}} + C_{\text{Naph,0}}}{1 + K_{\text{Mono}} + \dfrac{1}{K_{\text{Di}}} + \dfrac{1}{K_{\text{Di}} K_{\text{Poly}}}}. \tag{40}$$

Using another FORTRAN program, the values of $C_{\text{Mono},e}$, $C_{\text{Di},e}$, $C_{\text{Poly},e}$ and $C_{\text{Tot},e}$ at different temperatures have been determined using Eqs. 34, 35, 39, and 40, respectively. The equilibrium conversions have been calculated using Eqs. 28 through 31.

Results and Discussions

In Figure 2, the equilibrium constants have been plotted on a logarithmic scale against the absolute reaction temperature. It is evident from the figure that the equilibrium constants decrease with the temperature. The plot shows that at higher temperatures, $K_{\text{Poly}} > K_{\text{Di}} > K_{\text{Mono}}$, in contrast to their ranking at lower temperatures, that is, $K_{\text{Mono}} > K_{\text{Di}} > K_{\text{Poly}}$. Although this contradicts what has been reported in some of the literature, a similar trend supported by experimental observation has also been presented in Girgis and Gates (1991) and Stanislaus and Cooper (1994).

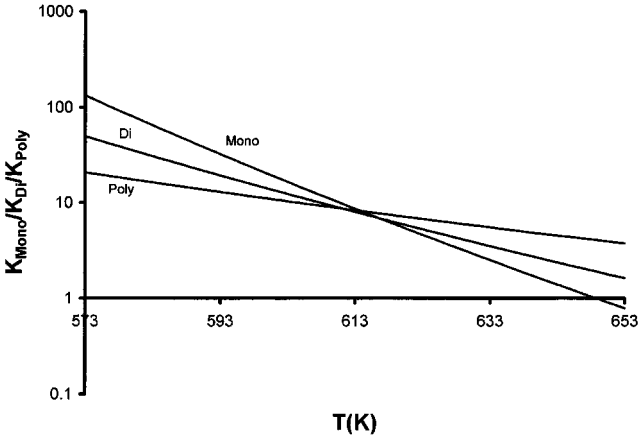

Figure 2. Equilibrium constants for hydrogenation reactions of mono-, di- and polyaromatics varied with temperature.

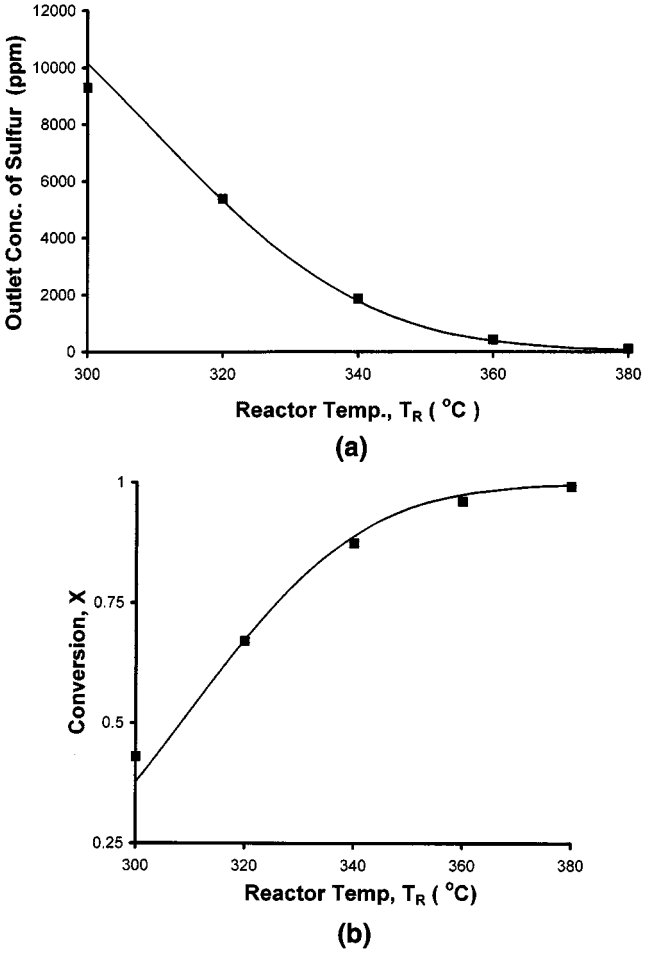

Figure 3. Simulated (lines) and experimental (points) variation of: (a) outlet sulfur content vs. reactor temperature; (b) conversion of sulfur compounds vs. reactor temperature.

$P = 4$ MPa, LHSV = 2.0 h^{-1}, $Q_g/Q_l = 200$ m^3/m^3, $y_{H_2S} = 1.4\%$.

In Figures 3a and 3b the concentration of product sulfur and the conversion of sulfur have been plotted against reactor temperature, respectively. With the increase in temperature the concentration of product sulfur decreases, and hence the conversion of sulfur compounds increases. Figures 3a and 3b show that for the present reaction temperature range ($300°C \le T_R \le 380°C$), the desulfurization is very well represented (correlation coefficient = 0.9 for Figure 3a and 0.98 for Figure 3b) by the model. It can be concluded that an irreversible reaction (assumption 7), following a Langmuir-

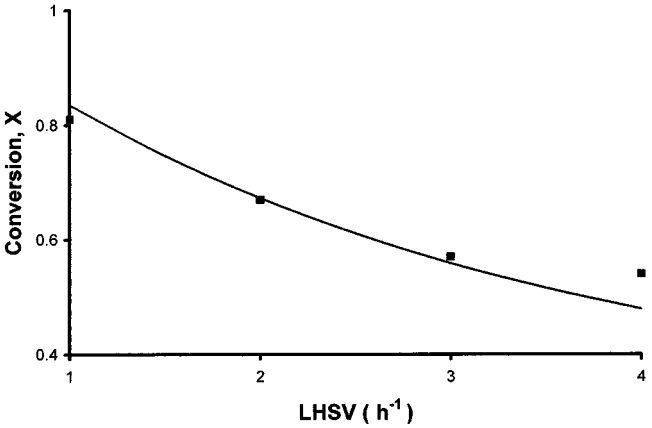

Figure 4. Simulated (lines) and experimental (points) variation of conversion of sulfur compounds vs. LHSV.

$P = 4$ MPa, $T_R = 320$°C, $Q_g/Q_l = 200$ m^3/m^3, $y_{H_2S} = 1.4\%$.

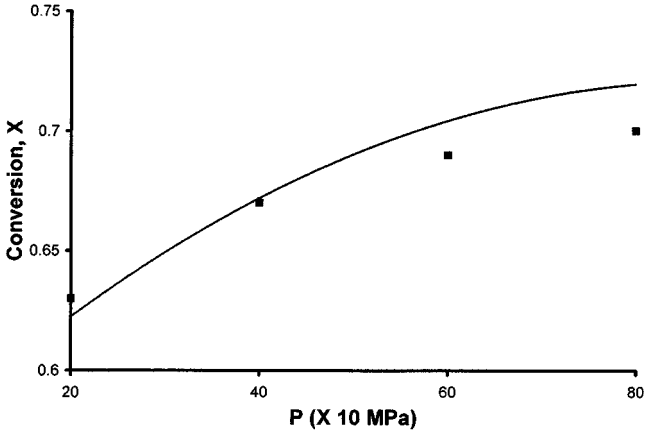

Figure 6. Simulated (lines) and experimental (points) variation of conversion of sulfur compounds vs. reactor pressure.

$T_R = 320$°C, LHSV = 2.0 h^{-1}, $Q_g/Q_l = 200$ m^3/m^3, $y_{H_2S} = 1.4\%$.

type rate expression, can represent very well the desulfurization under the present condition of study. This also proves the validity of the Arrhenius equation for the temperature dependence of the irreversible reaction rate constant and the constancy of the adsorption rate constant with temperature.

Figure 4 shows the dependence of the desulfurization of diesel oil on LHSV. With the decrease in LHSV, the conversion of sulfur compounds increases. The satisfactory agreement (correlation coefficient = 0.96) between the measured data and the model predictions in Figure 4 again justifies the Langmuir-type kinetic rate expression for representing desulfurization under the present study conditions.

In Figures 5 and 6, the conversion of sulfur compounds in diesel oil has been plotted against the gas-to-oil volumetric flow-rate ratios and pressure, respectively. The conversion increases constantly with the increase of both the Q_g/Q_l ratio and the reaction pressure. The experimental points have been plotted in the same figure. Close observation of the figure reveals that in reality the dependence of the conversion on the gas-to-oil volumetric flow-rate ratio is greater than that predicted by the present model. This deviation (correlation coefficient = 0.9) may be caused by the fact that the correlations used to determine the mass-transfer coefficients and Henry's law constants are not fully adequate for the system under study. The assumption that diesel oil only vaporizes at the entrance of the reactor may also cause the deviation. From a close analysis of Figure 6, which shows the effect of reaction pressure on sulfur conversion, it is evident that—probably for the same reasons as for the variation in the gas-to-oil volumetric flow-rate ratio—the agreement between the simulated and the experimental values shows little deviation (correlation coefficient = 0.93).

In Figure 7 the conversion of sulfur has been plotted against the initial concentration of H_2S in the gas-phase reactant. The experimental results have been superimposed on the

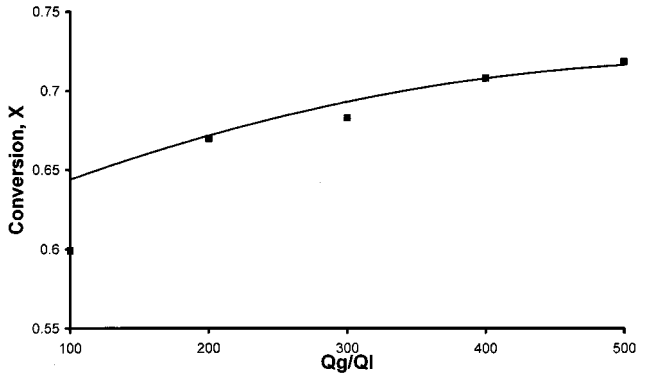

Figure 5. Simulated (lines) and experimental (points) variation of conversion of sulfur compounds vs. gas to oil volumetric flow rate ratio.

$P = 4$ MPa, LHSV = 2.0 h^{-1}, $T_R = 320$°C, $y_{H_2S} = 1.4\%$.

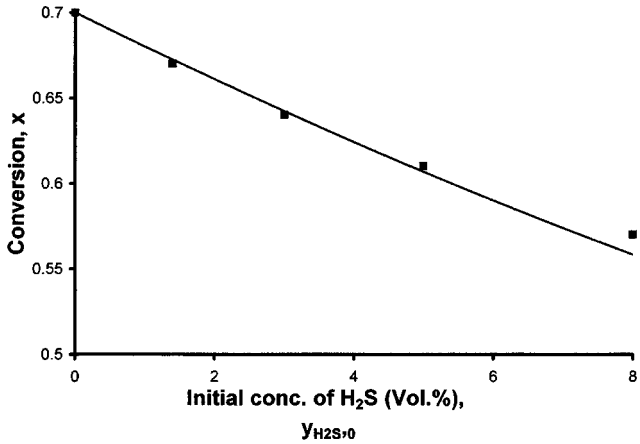

Figure 7. Simulated (lines) and experimental (points) variation of conversion of sulfur compounds vs. initial concentration (vol %) of H_2S in the reactant gas stream.

$P = 4$ MPa, LHSV = 2.0 h^{-1}, $Q_g/Q_l = 200$ m^3/m^3, $T_R = 320$°C.

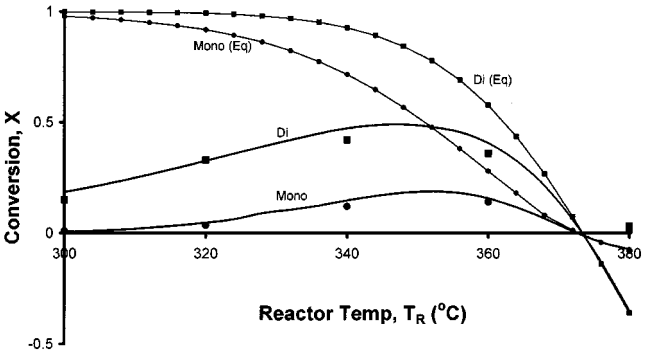

Figure 8. Simulated (lines) and experimental (points) variation of conversion and that of simulated equilibrium conversion of mono- and diaromatics vs. reactor temperature.

$P = 4$ MPa, LHSV = 2.0 h^{-1}, $Q_g/Q_l = 200$ m^3/m^3, $y_{H_2S} =$ 1.4%.

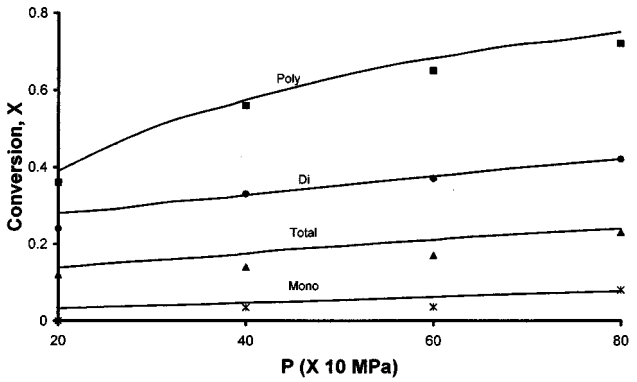

Figure 10. Simulated (lines) and experimental (points) variation of conversion of all aromatic compounds vs. reactor pressure.

$T_R = 320$°C, LHSV = 2.0 h^{-1}, $Q_g/Q_l = 200$ m^3/m^3, $y_{H_2S} =$ 1.4%.

same figure. The extent of desulfurization becomes less with the increase in the initial concentration of hydrogen sulfide in the reactant gas stream. Therefore, it is evident that the desulfurization reaction of diesel oil is inhibited by the presence of H_2S in the reactant gas stream. The simulated results replicate the reality satisfactorily (correlation coefficient = 0.98). The Langmuir-type kinetic equation with the temperature-independent adsorption coefficient, k_{ad}, is thus valid under the present experimental condition.

Figure 8 shows both the simulated and the actual effect of temperature on the conversion of mono- and diaromatics. Figure 9 shows the same effect for poly- and total aromatics. Although high conversion has been obtained for polyaromatics, the conversion of monoaromatics has been observed to be very difficult under the present reaction conditions. For all the components, the extent of the hydrogenation of aromatics increases when the temperature increases up to 360°C. Above this temperature, the extent of dearomatization becomes less. This may be explained by the fact that at higher temperatures the equilibrium is approached and the backward reactions become as fast as the forward reactions. This phenomenon has been clarified by plotting the equilibrium conversion curves for all the components. From the figures it is evident that at each temperature except the higher ones, the conversion is lower than for the equilibrium conversions using this NiMo catalyst.

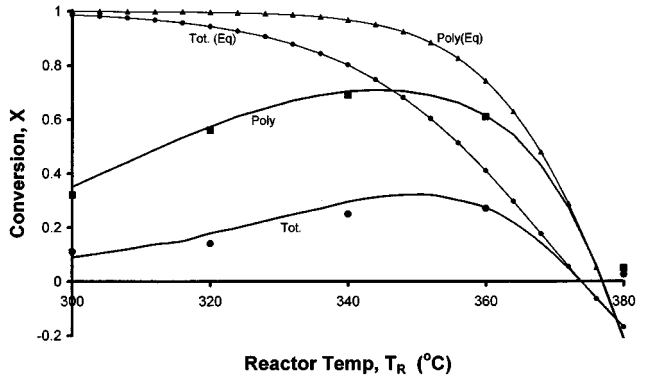

Figure 9. Simulated (lines) and experimental (points) variation of conversion and that of simulated equilibrium conversion of poly- and total aromatics vs. reactor temperature.

$P = 4$ MPa, LHSV = 2.0 h^{-1}, $Q_g/Q_l = 200$ m^3/m^3, $y_{H_2S} =$ 1.4%.

The model predicts a negative conversion for all components at 380°C, and it predicts zero conversion for all the components in the 375–380°C temperature range. However, experimental observations for all types of aromatics at 380°C indicated zero conversion. Although a temperature-controlled heater was used in the reactor, a deviation of ±3°C was always noticed, and hence a sharp decrease in conversion from zero to negative regime within 5°C might not be reflected in the experimental results. The negative conversion of aromatics at high temperatures was also reported by other investigators (Cooper et al., 1993). From an overall analysis of the figures, it is evident that the agreement between the experimental and simulated data is satisfactory (correlation coefficient = 0.92).

In Figure 10 both the simulated and experimental values of the aromatics conversions have been plotted against reaction pressure. For all the reactants, conversion increases with the increase in pressure under the present range of study. At the lowest pressure, namely, 2 Mpa, the conversion of monoaromatics tends to zero. Even the negative conversion of monoaromatics during conventional hydrogenation of diesel oil under low pressure has been reported (Stanislaus and Cooper, 1994). The mathematical model predicts the experimental trend satisfactorily. However, all aromatics conversion is overpredicted as a function of pressure. This overpredicting may be due to the simplistic representation of a complex reaction array. The pseudo-first-order assumption of the forward reaction, and the treatment of tri- and other polyaromatics as a single group of compounds in the mathematical model, are some of the examples. The deviation is, however, small (correlation coefficient = 0.96).

Figure 11 shows the simulated and actual dependence of the aromatics conversion on the LHSV. The conversion de-

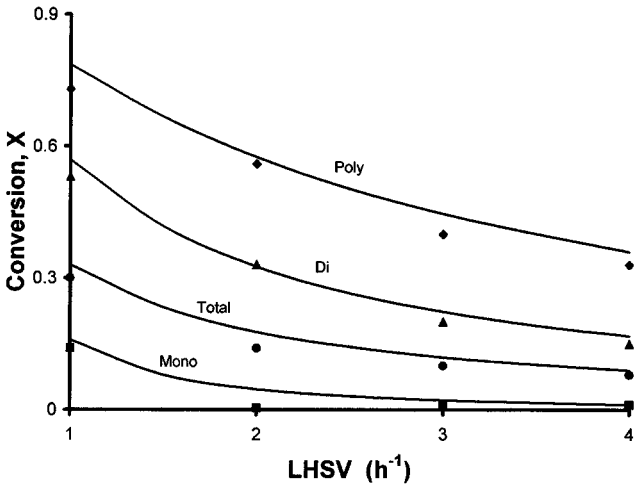

Figure 11. Simulated (lines) and experimental (points) variation of conversion of all aromatic compounds vs. LHSV.

$P = 4$ MPa, $T_R = 320$°C, $Q_g/Q_l = 200$ m^3/m^3, $y_{H_2S} = 1.4\%$.

creases with the increase in LHSV. At high values of LHSV (≥ 3.0 h^{-1}), the conversion of monoaromatics approaches zero. In some cases, negative conversion of monoaromatics at high values of LHSV has also been reported (Nash, 1989). The simulated trend is in good agreement with the experimental one. In each case, however, a little (correlation coefficient $= 0.98$) overprediction of conversion is noticed. The reason may be the same as in case of the dependence of pressure.

Acknowledgment

The work in this article was carried out at the Engler-Bunte-Institut, Germany.

The first author is highly grateful to DAAD (German Academic Exchange Service) for their financial support to carry out her research work in Germany. She is grateful to Prof. P. Bhattacharya of the Chemical Engineering Department, Jadavpur University, for his technical advice in revising the original manuscript. The authors are also indebted to the reviewers for their careful reading and critique of their original manuscript.

Notation

a_p = specific surface area, m^{-1}
Ar-S = aromatic sulfur compound
C = concentration, kmol/m^3
H = Henry's Law constant, MPa·m^3/kmol
ΔH = heat of reaction, kJ/kmol
k = reaction rate constant of desulfurization reaction, (m^3)$^{2.16}$/kg (kmol)$^{1.16}$·s
k^* = forward pseudo-first-order rate constant of dearomatization reactions, m^3/kg·s
k_- = backward rate constants of dearomatization reactions, m^3/kg·s
K = dynamic equilibrium constant, dimensionless
k_{ad} = adsorption coefficient, m^3/kmol
k^l = mass-transfer coefficient, m/s
$m1$ = order of desulfurization reaction with respect to aromatic sulfur compounds
$m2$ = order of desulfurization reaction with respect to hydrogen
$n1, n2, n3$ = order of dearomatization reactions with respect to hydrogen pressure
P = reaction pressure, MPa
Q = volumetric flow rate, m^3/s
R = gas-law constant, kJ/kmol·K
r = rate of heterogeneous reaction, kmol/kg·s
T = temperature, K or°C
u = superficial velocity, m/s
V = volume, m^3
X = fractional conversion, dimensionless
y = volume percent
z = axial coordinate along the length of the reactor, m

Greek letters

ϵ = void fraction, dimensionless
ξ = fractional volume of catalyst in the packed reactor bed, $[V_{cat}/(V_{cat} + V_{inert})]$, dimensionless
ρ_b = bulk density of the catalyst, kg/ m^3

Subscripts

cat = of catalyst
Di = of diaromatic
g = of gas phase
H_2 = of hydrogen
H_2S = of hydrogen sulfide
inert = of inert
l = of liquid phase
Mono = of monoaromatic
Naph = of naphthene
NTP = at NTP
Poly = of polyaromatic
R = of reactor
Tot = of total aromatic
$,e$ = at equilibrium
$,0$ = initial condition

Superscript

l = liquid phase

Literature Cited

Al-Dahhan, M. H., and M. P. Dudukovic, "Catalyst Bed Dilution for Improving Catalyst Wetting in Laboratory Trickle-Bed Reactors," *AIChE J.*, **42**, 2594 (1996).

Andari, M. K., F. Abu-Seedo, A. Stanislaus, and H. M. Qabazard, "Kinetics of Individual Sulfur Compounds in Deep Hydrodesulfurization of Kuwait Diesel Oil," *Fuel*, **75**, 1664 (1996).

Cooper, B. H., P. Sogaard-Andersen, and P. N. Hannerup, "Reduction of Aromatics in Diesel," *Oil Gas J.*, 95 (1992).

Cooper, B. H., A. Stanislaus, and P. N. Hannerup, "Hydrotreating Catalysts for Diesel Aromatics Saturation," *Hydrocarbon Process.*, 83 (1993).

Ertl, G., H. Knozinger, and J. Weitkamp, *Handbook of Heterogeneous Catalysis*, Vol. l4, Wiley-VCH, Weinheim, Germany (1996).

Girgis, M. J., and B. C. Gates, "Reactivities, Reaction Networks and Kinetics in High-Pressure Catalytic Hydroprocessing," *Ind. Eng. Chem. Res.*, **30**, 2021 (1991).

Huang, T. C., and B. C. Kang, "Kinetic Study of Naphthalene Hydrogenation Over Pt/Al_2O_3 Catalyst," *Ind. Eng. Chem. Res.*, **34**, 1140 (1995).

Jaffe, S. B., "Kinetics of Heat Release in Petroleum Hydrogenation," *Ind. Eng. Chem., Process. Des. Dev.*, **13**, 34 (1974).

Korre, S. C., M. Neurock, M. T. Klein, and R. J. Quann, "Hydrogenation of Polynuclear Aromatic Hydrocarbons. 2. Quantitative Structure/Reactivity Correlations," *Chem. Eng. Sci.*, **49**, 4191 (1994).

Korsten, H., and U. Hoffmann, "Three-Phase Reactor Model for Hydrotreating in Pilot Trickle-Bed Reactors," *AIChE J.*, **42**, 1350 (1996).

Levenspiel, O., *Chemical Reaction Engineering*, Wiley Eastern, New Delhi (1982).
Ma, X., K. Sakanishi, and I. Mochida, "Hydrodesulfurization Reactivities of Various Sulfur Compounds in Diesel Fuel," *Ind. Eng. Chem. Res.*, **33**, 218 (1994).
Ma, X., K. Sakanishi, T. Isoda, and I. Mochida, "Hydrodesulfurisation Reactivities of Narrow-Cut Fractions in a Gas Oil," *Ind. Eng. Chem. Res.*, **34**, 748 (1995).
Matarrese, G., E. Santoro, R. Covini, and F. Pignataro, "Process Conditions Are Important in Dearomatizing Gas Oil," *Oil Gas J.*, 111 (1983).
Nash, R. M., "Process Conditions and Catalyst for Low-Aromatics Diesel Studied," *Oil Gas J.* (Special Edition), 47 (1989).
Quann, R. J., and S. B. Jaffe, "Structure-Oriented Lumping: Describing the Chemistry of Complex Hydrocarbon Mixtures," *Ind. Eng. Chem. Res.*, **31**, 2483 (1992).
Quann, R. J., and S. B. Jaffe, "Building Useful Models of Complex Reaction Systems in Petroleum Refining," *Chem. Eng. Sci.*, **51**, 1615 (1996).
Sharma, S. D., K. Gadgil, and M. K. Sarkar, "Estimation of Kinetic Parameters of Benzene Hydrogenation in a Trickle Bed Reactor," *Chem. Eng. Technol.*, **16**, 347 (1993).
Sie, S. T., "Scale Effects in Laboratory and Pilot-Plant Reactors for Trickle-Flow Processes," *Rev. Linst. Fr. Pet.*, **46**, 501 (1991).
Stanislaus, A., and B. H. Cooper, "Aromatic Hydrogenation Catalysis: A Review," *Catal. Rev. Sci. Eng.*, **36**, 75 (1994).
Suchanek, A. J., "Catalytic Routes to Low-Aromatics Diesel Look Promising," *Oil Gas J.*, 109 (1990).
Valerius, G., X. Zhu, and H. Hofmann, "Modelling of a Trickle-Bed Reactor I. Extended Definitions and New Approximations," *Chem. Eng. Process.*, **35**, 1 (1996).
van den Berg, J. P., J. P. Lucien, G. Germaine, and G. L. B. Thielemans, "Deep Desulfurisation and Aromatics Saturation for Automotive Gasoil Manufacturing," *Fuel Process. Technol.*, **35**, 119 (1993).
Wilson, M. F., and J. F. Kriz, "Upgrading of Middle Distillate Fractions of a Syncrude from Athabasca Oil Sands," *Fuel*, **63**, 190 (1984).

Manuscript received Nov. 17, 2000, and revision received May 29, 2001.